Mon. Not. R. Astron. Soc. **292,** 27–42 (1997)

Equation of state of the photoionized intergalactic medium

Lam Hui[1] and Nickolay Y. Gnedin[2]

[1]*NASA/Fermilab Astrophysics Center, Fermi National Accelerator Laboratory, Batavia, IL 60510, USA*
[2]*Department of Astronomy, University of California, Berkeley, CA 94720, USA*

Accepted 1997 June 18. Received 1997 May 12; in original form 1997 January 7

ABSTRACT

We develop an efficient method of studying the effects of reionization history on the temperature–density relation of the intergalactic medium in the low-density limit (overdensity $\delta \lesssim 5$). It is applied to the study of photo-reionization models in which the amplitude, spectrum and onset epoch of the ionizing flux, as well as the cosmology, are systematically varied. We find that the mean temperature–density relation at $z = 2$–4 is well approximated by a power-law equation of state for uniform reionization models. We derive analytical expressions for its evolution and exhibit its asymptotic behaviour: it is found that for sufficiently early reionization, imprints of reionization history prior to $z \sim 10$ on the temperature–density relation are washed out. In this limit the temperature at the cosmic mean density is proportional to $[\Omega_b h/\sqrt{\Omega_0}]^{1/1.7}$. While the amplitude of the radiation flux at the ionizing frequency of H I is found to have a negligible effect on the temperature–density relation as long as the universe reionizes before $z \sim 5$, the spectrum can change the overall temperature by about 20 per cent, through variations in the abundances of helium species. However, the slope of the mean equation of state is found to lie within a narrow range for all reionization models we study, where reionization takes place before $z \sim 5$. We discuss the implications of these findings for the observational properties of the Lyα forest. In particular, uncertainties in the temperature of the intergalactic medium, arising from the uncertain reionization history of our Universe, introduce a 30 per cent scaling in the amplitude of the column density distribution while the slope of the distribution is only affected by about 7 per cent. Finally, we discuss how a fluctuating ionizing field affects the above results. We argue that under certain conditions, the loss of memory of reionization history implies that at late times, the temperature–density relation of a gas in a fluctuating ionizing background can be approximated by one that results from a uniform radiation field, provided the universe reionizes sufficiently early.

Key words: equation of state – intergalactic medium – quasars: absorption lines – cosmology: theory.

1 INTRODUCTION

Absorption-line studies of the low column density Lyα forest ($N_{\rm H\,I} \lesssim 15$ cm^{-2}: see Hu et al. 1995; Lu et al. 1996; Cristiani et al. 1997) offer a unique probe of the universe, which is free of luminosity bias, spans a wide redshift range $z \sim 2$–4 and where the overdensity is mildly non-linear (overdensity $\delta \lesssim 5$, see Hui, Gnedin & Zhang 1997) and hence the relevant physics is simple to understand. Recent hydrodynamic simulations support the hypothesis that the Lyα forest arises from a fluctuating intergalactic medium that is the natural result of gravitational instability in hierarchical clustering cosmological models (Cen et al. 1994; Zhang, Anninos & Norman 1995; Hernquist et al. 1996; Miralda-Escudé et al. 1996; Wadsley & Bond 1997).

The main quantity of interest in such studies is the Lyα transmission (or optical depth) as a function of frequency, which is determined by the density of neutral hydrogen as a function of position. The Gunn–Peterson effect (Gunn & Peterson 1965) tells us that hydrogen (as well as helium) is highly ionized for $z \lesssim 5$. Several models for its origin have been studied: photoionization by first generation of stars or quasars, collisional ionization induced by shock-heated gas, decaying neutrinos and so on (Ikeuchi & Ostriker 1986;

Couchman & Rees 1986; Sciama 1990; Miralda-Escudé & Ostriker 1992; Shapiro, Giroux & Babul 1994; Giroux & Shapiro 1996; Haiman & Loeb 1996). The reader is also referred to Shapiro (1995) for an excellent review on the subject. We focus on photoionization models in this paper although the semi-analytical method we propose in this paper can be applied to any model.

Ionization equilibrium, which should hold after the universe reionizes, dictates that the neutral hydrogen density is approximately proportional to $\rho_b^2 T^{-0.7}$ where ρ_b is the baryon density and T is the temperature (see Section 3.1.1). It is therefore important to know the amplitude of T and its dependence on ρ_b. As we will discuss later, the temperature–density relation can significantly affect observed properties of the Lyα forest, its column density distribution for instance.

Imagine a fluid element evolving in a photoionized intergalactic medium. Its temperature at $z \sim 2$–4 is influenced by a number of factors: how its density evolves with time, which determines the amount of heating/cooling; how and when the ionizing radiation is turned on; the radiation amplitude and spectrum, which control how much photoionization heating the fluid element suffers; cosmological parameters such as baryon density, the Hubble constant and the density parameter Ω_0 that affects the recombination rate, adiabatic cooling rate and the evolution of density.

The temperature–density relation for a set of fluid elements is then determined by, among other things, the reionization history of the universe. Given a reionization scenario and cosmological model, hydrodynamic simulations can predict this relation accurately, but limited computer resources obviously restrict the numer of reionization histories one can study. It is therefore important that we develop alternative tools in order to understand the effects of a full range of reionization histories, considering the as yet poor knowledge of the actual reionization history of our Universe. Moreover, it is worth pointing out that there exist analytical tools borrowed from studies of large-scale structure that can predict the distribution of ρ_b with reasonable accuracy in the low-density regime (Doroshkevich & Shandarin 1977; Bi, Borner & Chu 1992; Bi & Davidsen 1997; Gnedin & Hui 1996; Hui et al. 1997). By their analytical/semi-analytical nature, it is possible to study a whole range of cosmological models in an efficient manner. What remains to be specified for these methods, in order to calculate quantities like the column density distribution of hydrogen, is the temperature–density relation. A calculation aiming at just that is attempted here.

We propose to model the density evolution of each fluid element using the Zel'dovich approximation (Zel'dovich 1970), which is known to be a good approximation in the mildly non-linear regime (Coles, Melott & Shandarin 1993) and for elements where hydrodynamic effects like pressure and shock-heating are unimportant. Given a probability distribution of the initial configuration for these elements, which can be deduced for any given cosmological model, one can generate a whole set of such elements and simply follow their thermal and chemical evolution. The resulting bulk temperature–density relation can then be studied for any chosen reionization history. The virtue of this method is that each element can be treated independently and that the density evolution is given by an analytical formula (from the Zel'dovich approximation) while the thermal and chemical evolution equations involve a set of ordinary differential equations which can be solved numerically. Obviously, such a Lagrangian method does not incorporate the effects of shock heating properly. We check the results of our method against full hydrodynamic simulations and find good agreement for $\delta \lesssim 5$, implying shock effects are not significant in the low-density regime (Section 2.2).

Most previous work investigating the effects of different reionization histories either assumes a uniform intergalactic medium (e.g. Giroux & Shapiro 1996) or uses the spherical collapse model for density evolution (e.g. Miralda-Escudé & Rees 1994). For the low column density Lyα forest, which arises naturally from a mildly fluctuating intergalactic medium, and which hydrodynamic simulations indicate to be consisting mostly of filaments and pancakes (Cen et al. 1994), the density evolution is better approximated by the Zel'dovich approximation (Hui et al. 1997).

A great deal of effort has been made to examine radiative transfer effects after the onset of ionizing radiation, including the expansion of H II regions, reprocessing by absorption systems etc. (Zuo 1992a,b; Meiksin & Madau 1993; Miralda-Escudé & Rees 1994; Giroux & Shapiro 1996; Haardt & Madau 1996; see also Gnedin & Ostriker 1997 for numerical simulations that include some of these effects). These effects can in principle be incorporated in our method by specifying how the radiation intensity correlates with density and possibly allowing the onset of reionization to occur at different times for different fluid elements. While more work still needs to be carried out in order to make such a specification with reasonable accuracy, we focus in this paper on reionization models in which the ionizing flux is uniform, but allowing the onset-epoch, spectrum and amplitude of the ionizing flux as well as the cosmology to vary. It turns out one can learn something about the more realistic fluctuating case, even from these simple models, which we will discuss in Section 5.

As we will show, the mean temperature–density relation of the photoionized intergalactic medium in the low-density region is well-approximated by a power-law equation of state $[T \propto (1+\delta)^{\gamma-1}]$ where δ is the mass overdensity. The questions we would like to address are then: how does the amplitude and slope of the equation of state depend on the reionization history, characteristics of the ionizing radiation as well as cosmological parameters; what are the implications for observational properties of the Lyα forest?

Organization of the paper is as follows. In the next section, we outline a semi-analytical method to predict the temperature–density relation for any given cosmology and reionization history, using the Zel'dovich approximation. An example is discussed and a comparison is made with the result of a full hydrodynamic simulation, computed using the same reionization history. Then, in Section 3 we apply the method to study models in which the universe reionizes suddenly, owing to a rapid outburst of radiation. We investigate systematically how varying the epoch of reionization, cosmological parameters and the radiation amplitude and spectrum affects the equation of state at later redshifts. Analytical approximations to the equation of state are derived. In Section 4, it is shown that models in which reionization occurs after a period of reheating (gradual turn-on of radiation) give equations of state that can be

well-fitted by that of an appropriate sudden reionization model. Finally we discuss the implications of our findings for the observational properties of the Lyα forest and the intergalactic medium in Section 5. A summary of relevant reaction rates is provided in the Appendix.

A few words about our terminology. The three different methods or procedures to study the effects of reionization history are respectively referred to as 'analytical approximation', 'semi-analytical method' and 'hydrodynamic simulation'. The first is discussed in Section 3, where a few approximations are made to derive the equation of state in closed form; the second is explained in Section 2.1, which evolves the density analytically but requires numerical integration of the thermal and chemical evolution equations, although not a full scale hydrodynamic simulation and the third is what its name suggests. While the last method is perhaps the most accurate (provided the numerical resolution is sufficient), the second, which is the focus of this paper, allows us to study the temperature–density relation for a large number of reionization histories in an efficient and accurate manner, albeit restricted to the low-density regime; the first allows us to give useful approximate quantitative expressions that embody the correct qualitative trends. Standard symbols are used for cosmological parameters: $a=(1+z)^{-1}$ where $1+z$ is the cosmological redshift factor, H for the Hubble constant as a function of z, H_0 for the Hubble constant today, h for $H_0/100$ km s^{-1} Mpc^{-1}, Ω for the density parameter today, with the subscript b to denote its baryon portion and 0 all its matter content, and Λ for the contribution from cosmological constant. We use the symbol h (to be distinct from h) to denote the Planck constant in the few places where it arises and $k_{\rm B}$ to denote the Boltzmann constant.

2 THE SEMI-ANALYTICAL METHOD

2.1 The equations

In a nutshell, the method we propose is very simple: assume that the density evolution of a given fluid element is governed by the Zel'dovich approximation; allow the element to cool/heat and its constituents to change according to standard thermal and chemical reaction rates; repeat the same procedure for a whole set of fluid elements with initial parameters drawn from a distribution implied by whatever cosmological initial conditions one prefers (in this paper, we study only Gaussian random initial conditions). The resulting temperature–density relation can be obtained by making a scatter-plot of temperature versus density for all the fluid elements at a given time of interest.

The density evolution of a fluid element, according to the Zel'dovich approximation, is given by

$$1+\delta=\det{}^{-1}[\delta_{ij}+D_+(t)\psi_{ij}], \qquad (1)$$

where δ is the mass overdensity, δ_{ij} is the Kronecker delta and $D_+(t)$ is the linear growth factor (Peebles 1980), the time dependence of which is completely specified by cosmology (e.g. it equals the Hubble scalefactor a for a universe at critical matter density). The normalization is chosen such that $D_+=1$ today.

The tensor ψ_{ij} is a 3×3 symmetric matrix determined by initial conditions (i.e. its components vary from one fluid element to another). One can always choose a basis in which the matrix is diagonal. So, the problem of initial conditions reduces to finding the probability distribution of its three eigenvalues. This problem was solved by Doroshkevich (1970) for Gaussian random initial density field, (see also Bartelmann & Schneider (1992) for an elegant alternative derivation) which we also assume in this paper. For recent discussions of how to generate realizations of matrix ψ_{ij}, see Bertschinger & Jain (1994) and Reisenegger & Miralda-Escudé (1995). It can be shown that the probability distribution of the matrix ψ_{ij} is uniquely specified by the dispersion of its trace. In the limit where $D_+(t)$ is small, it can be seen that the trace multiplied by $-D_+(t)$ is equal to δ, i.e. the linear overdensity. Therefore, the average of the trace vanishes and its rms (root mean squared) value is equal to the rms linear density fluctuation today, σ. At a given redshift and for a fixed number of fluid elements, a given rms σ value would imply a probable range of δs in which most elements will end up. For the range we are interested in (δ between about -0.9 and 5, at z from 2 to 4), we find that setting the rms value σ to 2 is adequate. For a fixed number of fluid elements, choosing a higher value for σ has the effect of shifting the probable range of densities upward and also increasing the scatter in a plot of temperature versus density. Alternatively, for a fixed rms value σ, one can reproduce this latter effect and increase the number of fluid elements that fall in the desired density range by increasing the total number of fluid elements in a realization. We find that for our densities and redshifts of interest, using a different σ does not change the overall temperature–density relation significantly. However, it should be kept in mind the scatter in temperature–density relation is limited, in part, by the finite number of elements in the realizations.

Temperature obeys the following equation of evolution:

$$\frac{{\rm d}T}{{\rm d}t}=-2HT+\frac{2T}{3(1+\delta)}\frac{{\rm d}\delta}{{\rm d}t}-\frac{T}{\Sigma_i\tilde{X}_i}\frac{{\rm d}\Sigma_i\tilde{X}_i}{{\rm d}t}+\frac{2}{3k_{\rm B}n_{\rm b}}\frac{{\rm d}Q}{{\rm d}t}, \qquad (2)$$

where ${\rm d}/{\rm d}t$ is the Lagrangian derivative following each fluid element, $n_{\rm b}$ is the proper number density of all gas particles (i.e. everything except non-interacting dark matter) and T is the temperature which depends on both space and time. The symbol $\tilde{X}_i$ is defined by $n_i\equiv(1+\delta)\tilde{X}_i\bar{\rho}_{\rm b}/m_{\rm p}$, where n_i is the proper number density of the species i, $\bar{\rho}_{\rm b}$ is the mean mass density of baryons at the time of interest and $m_{\rm p}$ is the mass of the proton and δ is the mass overdensity. For example the neutral fraction of hydrogen, $X_{\rm H\,I}$ (to be distinguished from $\tilde{X}_{\rm H\,I}$), is then $\tilde{X}_{\rm H\,I}/(\tilde{X}_{\rm H\,I}+\tilde{X}_{\rm H\,II})$. Note that $\tilde{X}_i$ is a function of space and time in general.

The first two terms on the right-hand side take care of adiabatic cooling or heating. The third accounts for the change of internal energy per particle resulting from the change in the number of particles. The last term ${\rm d}Q/{\rm d}t$ is the heat gain (or negative heat loss) per unit volume by the gas particles from the surrounding radiation field. The heating and cooling rates owing to photoionization, recombination and Compton scattering are summarized in the Appendix.

Equation (2) has to be supplemented by one that determines the abundance of each particle type, which takes the form

$$\frac{{\rm d}\tilde{X}_i}{{\rm d}t}=-\tilde{X}_i\Gamma_i+\sum_{j,k}\tilde{X}_j\tilde{X}_kR_{jk}\left[\frac{\bar{\rho}_{\rm b}(1+\delta)}{m_{\rm p}}\right], \qquad (3)$$

where Γ_i is the photoionization rate of the species i and R_{jk} is the recombination rate (in units of volume per unit time) of the species j and k to give i. The photoionization rate is given by

$$\Gamma_i = \int_{\nu_i}^{\infty} 4\pi J_\nu \sigma_i \frac{d\nu}{h\nu}, \tag{4}$$

where J_ν is the specific intensity of the ionizing radiation as a function of frequency ν, ν_i is the frequency above which a photon can ionize the species i and σ_i is the cross-section for this process. The cross-sections for different species as well as the recombination rates are given in the Appendix.

What remains to be specified in the time evolution of the specific intensity of the ionizing radiation as a function of frequency, which determines the photoionization (Γ_i) and photoionization heating (dQ/dt) rates. We will examine the effects of a wide range of amplitudes, spectra and time evolution of the ionizing radiation in this paper.

Equations (1), (2) and (3) completely determine the thermal and chemical evolution of a fluid element. They are numerically integrated for each fluid element with the initial condition for δ determined as discussed before. The thermal and chemical initial conditions are chosen as follows. The gas temperature T is equal to the cosmic microwave background temperature at $1+z=100(\Omega_b h^2/0.0125)^{2/5}$ (maintained by Compton scattering; Peebles 1993) and evolves adiabatically after that until the Universe is reionized by the UV background. Abundances are assumed to be primordial, which is consistent with current observations in the low-density intergalactic medium. All species are neutral to high accuracy until reionization occurs. One can integrate equations (2) and (3) forward starting from any time between $z=100$ and the beginning of reionization.

2.2 Comparison with hydrodynamic simulation

We show in Fig. 1 scatter plots of temperature versus density at $z=4$ obtained using the semi-analytical method outlined above and using a full hydrodynamic simulation respectively. The same uniform ionization field has been used for both of them, the evolution of which is shown in Fig. 2.[1] The radiation field is computed in a hydrodynamic simulation that includes the effects of star formation (see Gnedin & Ostriker 1997). In Fig. 2, we quantify the level of the ionizing radiation by the photoionization rates it implies, i.e.

$$J_i = \frac{\int_{\nu_i}^{\infty} 4\pi J_\nu \sigma_i \, d\nu/\nu}{\int_{\nu_i}^{\infty} 4\pi \sigma_i \, d\nu/\nu} (10^{-21} \text{ erg Hz}^{-1} \text{ s}^{-1} \text{ cm}^{-2} \text{ sr}^{-1})^{-1}, \tag{5}$$

where the notations are the same as those defined in equation (4). For instance, $J_{\rm H\,I}$ is related to the photoionization rate of neutral hydrogen $\Gamma_{\rm H\,I}$ by $\Gamma_{\rm H\,I} \sim 4\times10^{-12} J_{\rm H\,I}\,\text{s}^{-1}$ (more accurate proportionality constant can be inferred from the cross-section $\sigma_{\rm H\,I}$ given in our Appendix). The three different quantities $J_{\rm H\,I}$, $J_{\rm He\,I}$ and $J_{\rm He\,II}$ shown in Fig. 2 do not completely specify J_ν, but they give an indication of how J_ν changes with time at different frequencies. The full spectrum of J_ν is of course known and used in producing the results shown in Fig. 1 but we do not show it here. (In practice, one actually needs only three more pieces of information regarding J_ν for the thermal evolution of a gas of primordial composition: the photoionization *heating* rates of H I, He I and He II.)

[1]See Section 5 for a discussion of the effect of a non-uniform radiation field.

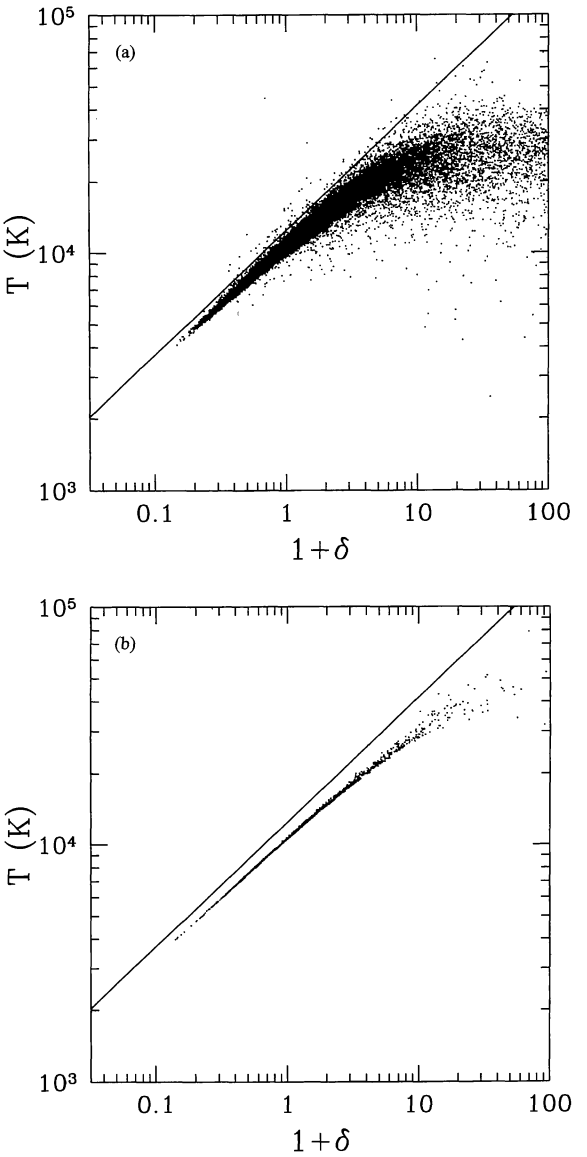

Figure 1. A scatter-plot (black dots) of temperature versus density of 40 000 cells randomly drawn from a 64^3 CDM + Λ hydrodynamic at $z=4$ using the SLH-P^{3}M algorithm (see Gnedin 1995 and Gnedin & Bertschinger 1996) with $\Omega_0=0.35$, $\Omega_\Lambda=0.65$, $\Omega_b=0.055$ and $h=0.7$ (left panel). The evolution of the ionizing background for the simulation is shown in Fig. 2. The right panel shows the temperature–density relation obtained for exactly the same cosmological and radiation parameters using the semi-analytical method described in Section 2.1, applied to 2000 fluid elements. The larger scatter in (a) compared to (b) is in part due to the smaller number of elements in the latter. The solid line plotted in both figures corresponds to the analytical approximation expressed in equations (13), (19) and (22) for a sudden reionization model where the epoch of reionization is $1+z=9$.

Our simple semi-analytical method gives a temperature–density relation that is well approximated by a power law for

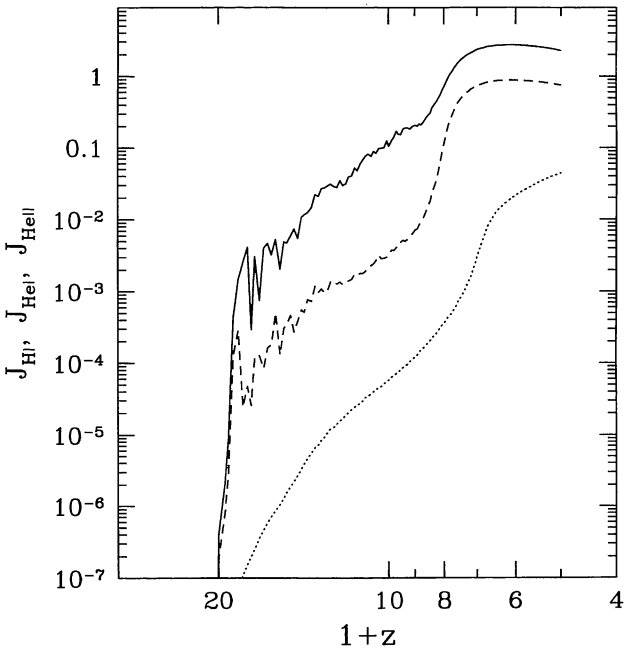

Figure 2. Evolution of $J_{\rm H\,I}$ (solid line), $J_{\rm He\,I}$ (dashed line) and $J_{\rm He\,II}$ (dotted line) as a function of redshift, used in the computations shown in Fig. 1. The J_is are defined in equation (5).

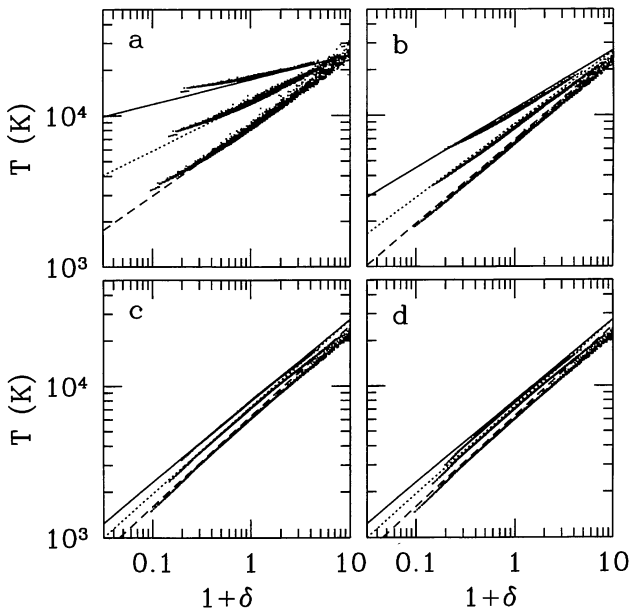

Figure 3. The temperature–density relation for 4 different sudden-reionization models: sudden reionization (see equation 6) at $z=5$ (a), $z=7$ (b), $z=10$ (c) and $z=10$ (d). For each reionization model, the black dots shown are the results of calculations using the semi-analytical method outlined in Section 2.1 for 2000 elements, shown at three different instants: z being 4, 3 and 2 from top to bottom. The cosmological parameters are $h=0.5$, $\Omega_0=1$ and $\Omega_b h^2=0.0125$ (with primordial abundances for hydrogen and helium). The ionizing background is specified by its amplitude $J_{\rm H\,I}=0.5$ (equation 5) and spectrum obeying equation (7) with $f=0.01$. The solid, dotted and dashed lines, from top to bottom for each reionization model, represent the analytical expressions for the equation of state in equations (13), (19) and (22), using the corresponding cosmological parameters and reionization-epoch for each model. The only exception is panel (d) where the lines shown are exactly the same as those in the panel (c), i.e. setting $a_{\rm reion}=1/11$ in equations (19) and (22) (see explanation in the text).

$\delta \lesssim 5$. It gives the correct mean behaviour of gas elements in the full hydrodynamic simulation in the low-density regime. The larger scatter in Fig. 1(a) compared with 1(b) is in part because of the smaller number of fluid elements in the latter. At higher densities, one begins to see the effect of shocks: a wide scatter of temperature at a fixed density. The calculation shown in Fig. 1(b) is not reliable in this regime. This is because by assuming that density evolves as prescribed by the Zel'dovich approximation, which is only a good approximation for pressureless (dark) matter or baryons at large scales, one misses the effects of gas pressure and shocks as the fluid element is compressed to sufficiently high densities. Note also that the temperature of gas elements at a high density tends to be higher in the approximate semi-analytical calculation compared to the full hydrodynamic computation. This might seem counter-intuitive since shock heating is properly taken into account in the latter but not the former. There are two reasons. First, because of the small box size of the hydrodynamic computation, large-scale power and, hence, shock heating is suppressed in Fig. 1(a). Secondly, the Zel'dovich approximation breaks down beyond shell crossing, and so in Fig. 1(b), we include only those elements that have not shell crossed. This means that at a given final high density, an element in Fig. 1(b) should be just about to shell cross while a typical element in Fig. 1(a) has probably done so already and is expanding, allowing for more cooling. Both of the above effects explain the relatively low temperature at a high density of the hydrodynamic simulation compared to our approximate semi-analytical calculation. We are, of course, interested in only the temperature–density relation in the low-density regions ($\delta \lesssim 5$), where the two methods agree very well.

We have made a number of similar comparisons between the temperature–density relations obtained from hydrodynamic simulations versus using our semi-analytical method, for a number of different J_νs as a function of time. The semi-analytical method consistently gives the correct mean behaviour of gas elements of low density. Keeping in mind the intrinsic scatter such as that seen in Fig. 1(a), we can make use of our simple semi-analytical method to efficiently study the mean temperature–density relation at the low-density regime for a large number of reionization scenarios, which is the subject of the next two sections.

3 SUDDEN REIONIZATION MODELS

3.1 Variation with the epoch of reionization

In Fig. 3 we show the temperature–density relation for four different sudden reionization models, where the reionization epoch is systematically varied. All of them have no ionizing background until the specified epoch and then $J_{\rm H\,I}$ (equation 5) is taken to be 0.5 thereafter, i.e.

$$J_{\rm H\,I}=\begin{cases} J_{\rm ion} & \text{for } a \geq a_{\rm reion}, \\ 0 & \text{for } a < a_{\rm reion}, \end{cases} \qquad (6)$$

where $a_{\rm reion}=(1+z_{\rm reion})^{-1}$ is the Hubble scalefactor when the radiation is turned on and the parameter $J_{\rm ion}$ is chosen to be 0.5 (we will study the effects of varying $J_{\rm ion}$ later on).

It is assumed that $J_\nu \propto \nu^{-1}$, except that it suffers a factor of $f=0.01$ reduction beyond the frequency corresponding to the ionization of He II:

$$J_\nu = \begin{cases} J_0\left(\dfrac{\nu}{\nu_{\rm H\,I}}\right)^{-1} & \text{for } \nu \le \nu_{\rm He\,II}, \\ fJ_0\left(\dfrac{\nu}{\nu_{\rm H\,I}}\right)^{-1} & \text{for } \nu > \nu_{\rm He\,I}, \end{cases} \tag{7}$$

where J_0 is chosen so that $J_{\rm H\,I}$ (equation 5) has the desired value, $\nu_{\rm He\,II}$ is the frequency corresponding to the ionization of He II and f (now chosen to be 0.01) is a parameter specifying by how much the ionizing radiation is to be further diminished beyond $\nu_{\rm He\,II}$.

Ignoring for the time being the solid, dotted and dashed lines in Fig. 3 which will be discussed in the next section, the first trend to notice is that the earlier the epoch of reionization, the lower the overall temperature at a given redshift, except that for sufficiently early reionization ($z_{\rm reion}>10$), the temperature–density relation approaches an asymptote. The second, somewhat striking, result is how well the temperature–density relations are approximated by power-law equations of state, where the slope steepens as the universe reionizes earlier. The third is that when the reionization epoch is pushed sufficiently early, the exact time when it occurs makes very little difference to the equation of state: hence the very similar temperature–density relations for reionization starting at $z=10$ and 19 in Figs 3(c) and (d).

To understand these trends, we perform the following approximate analytical calculation.

3.1.1 *Analytical calculation*

First, let us determine the reionization temperature. In the limit when a substantial amount of radiation is suddenly turned on, one can approximate equations (2) and (3) by

$$\frac{{\rm d}T}{{\rm d}t} = -\frac{T}{\Sigma_i \tilde{X}_i}\frac{{\rm d}\Sigma_i \tilde{X}_i}{{\rm d}t} + \frac{2}{3k_{\rm B}}\frac{\tilde{X}_{\rm H\,I}}{\Sigma_i \tilde{X}_i} \times \int_{\nu_{\rm H\,I}}^{\infty} 4\pi J_\nu \sigma_{\rm H\,I}({\rm h}\nu - {\rm h}\nu_{\rm H\,I})\frac{{\rm d}\nu}{{\rm h}\nu}, \tag{8}$$

$$\frac{{\rm d}\tilde{X}_{\rm H\,I}}{{\rm d}t} = -\tilde{X}_{\rm H\,I}\int_{\nu_{\rm H\,I}}^{\infty} 4\pi J_\nu \sigma_{\rm H\,I}\frac{{\rm d}\nu}{{\rm h}\nu},$$

where we have used equation (4) and have taken the crude approximation that the only two processes which significantly affect the temperature under the short time-scale of reionization (reciprocal of photoionization rate) are photoionization heating of hydrogen:

$$\frac{{\rm d}Q}{{\rm d}t} \sim n_{\rm H\,I}\int_{\nu_{\rm H\,I}}^{\infty} 4\pi J_\nu \sigma_{\rm H\,I}({\rm h}\nu - {\rm h}\nu_{\rm H\,I})\frac{{\rm d}\nu}{{\rm h}\nu} \tag{9}$$

and the change in the total number of gas particles. Note that during this brief period of radiation turn-on, the abundances of various species are far from equilibrium.

To integrate the above equations, we adopt the further approximation that the universe has only hydrogen, i.e. the term $\Sigma_i \tilde{X}_i = 2 - \tilde{X}_{\rm H\,I}$. Putting $T=0$ right before reionization because the temperature right after is much higher, we obtain the large time limit of T:

$$T_{\rm reion} = \frac{1}{3k_{\rm B}}E_J,$$

$$E_J \equiv \left[\frac{\displaystyle\int_{\nu_{\rm H\,I}}^{\infty} 4\pi J_\nu \sigma_{\rm H\,I}({\rm h}\nu - {\rm h}\nu_{\rm H\,I})\,{\rm d}\nu/{\rm h}\nu}{\displaystyle\int_{\nu_{\rm H\,I}}^{\infty} 4\pi J_\nu \sigma_{\rm H\,I}\,{\rm d}\nu/{\rm h}\nu}\right], \tag{10}$$

where E_J is kept constant after the radiation field is turned on. This is the temperature that the intergalactic medium reaches asymptotically before recombination processes become important and halt the exponential decrease of $\tilde{X}_{\rm H\,I}$, setting its value to that implied by ionization equilibrium thereafter (hydrogen is now highly ionized). Making use of $J_\nu \propto \nu^{-1}$, it can be shown that $T_{\rm reion} \sim 20\,000$ K. This value is not significantly affected by the slope of J_ν assuming it is between -1 and -1.5 at frequencies immediately above $\nu_{\rm H\,I}$, nor by the behaviour of J_ν at still higher frequencies.

Therefore, the first conclusion to draw is that for sudden reionization models, the temperature of reionization is largely independent of $J_{\rm H\,I}$, density, the epoch of reionization or even cosmology. We checked this for a few fluid elements in the computations shown in Fig. 3 and found that it is indeed the case. One possible exception, which we will discuss in Section 3.3, is that changing the spectrum of J_ν can affect the helium abundance, which in turn has a non-negligible effect on $T_{\rm reion}$. For sufficiently high redshifts, $a_{\rm reion} \lesssim 1/15$, we also find $T_{\rm reion}$ to be a little less than the value given above, because of a non-negligible amount of Compton cooling.

Next, we consider the evolution of T from the epoch of reionization to $z=2$, 3 and 4. Judging from the result in Fig. 3 that for sufficiently early reionization, the temperature–density relation approaches an asymptote, it seems reasonable to assume that what matters is the dominant thermal and chemical reaction rates at the later redshifts. In this regime, the dominant heating mechanism is again the photoionization of neutral hydrogen, aside from adiabatic heating/cooling (recall that we assume a universe filled with only hydrogen). For sufficiently low temperature, recombination (of proton and electron) cooling is subdominant compared to photoionization heating (at a temperature of the order of 10^4 K, the recombination cooling rate is smaller but actually not negligible compared with photoionization heating; it is again a crude approximation we adopt to make the problem tractable analytically). Putting all these into equation (2), the thermal evolution is then approximated by

$$\frac{{\rm d}T}{{\rm d}t} = -2HT + \frac{2T}{3(1+\delta)}\frac{{\rm d}\delta}{{\rm d}t} + \frac{2}{3k_{\rm B}}\frac{\tilde{X}_{\rm H\,II}\tilde{X}_e}{\Sigma_i \tilde{X}_i}\frac{\bar{\rho}_{\rm b}}{m_{\rm p}}(1+\delta)RE_J, \tag{11}$$

where we have ignored the term in equation (2) resulting from the change in the number of species, used equations (4), (9) and (10) and assumed ionization equilibrium (setting the right-hand side of equation 3 to zero), with R approximately given by

$$R \approx 4.2 \times 10^{-13} \left(\frac{T}{10^4\ \mathrm{K}}\right)^{-0.7} \mathrm{cm^3\ s^{-1}}. \quad (12)$$

A more accurate expression for R is given in the Appendix and used for our semi-analytical computation but this approximate form suffices for the present analytical calculation. Moreover, assuming again there is only hydrogen in the Universe, we will approximate $\tilde{X}_{\mathrm{H_{II}}}\tilde{X}_e/\Sigma_i \tilde{X}_i$ by 1/2 (recall that hydrogen is now highly ionized).

Even with this highly simplified equation, the problem of predicting the temperature–density relation is still untractable analytically, if one uses the density evolution as expressed in equation (1).

The next best question to ask is then: given that the outcome is a power-law equation of state, can we at least predict its amplitude and slope? To do so, we turn to linear theory. We expand the logarithm of T to first order in δ:

$$\ln T = \ln T_0 + (\gamma - 1)\delta = \ln T_0 + (\gamma - 1)[\ln(1+\delta)], \quad (13)$$

where T_0 is simply the temperature of a fluid element that remains at the cosmic mean density and $\gamma - 1$ multiplied by δ gives the fluctuation about the mean (the notation $\gamma - 1$ is chosen to agree with the common notation as in equation 14). The second equality holds in the small δ limit. The power-law slope relating temperature and density for small δ is then given by $\mathrm{d}\ln T/\mathrm{d}\ln(1+\delta) = \gamma - 1$. Knowing that a single power-law equation of state approximately holds even for δ not very small, $\gamma - 1$ is then taken to be the correct power-law slope throughout our range of interest, i.e.

$$T = T_0 (1+\delta)^{\gamma - 1}. \quad (14)$$

Putting $\delta = 0$ into equation (11) and making use of the relation $H = H_0 \Omega_0^{1/2}(1+z)^{3/2}$ where Ω_0 is the ratio of matter density to critical density today (the expression is exact for $\Omega_0 = 1$ and approximately true at sufficiently high redshift; see Peebles 1993, chapter 5), it is possible to show that

$$\frac{\mathrm{d}a^2 T_0}{\mathrm{d}a} = T_0^{-0.7} a^{-1/2} B \quad (15)$$

where B is defined by

$$B \equiv \frac{\rho_{\mathrm{c}100}}{m_p} T_{\mathrm{reion}} R T_0^{0.7} \frac{\Omega_{\mathrm{b}} h^2}{H_0 \sqrt{\Omega_0}} \approx 11.4\ \mathrm{K}^{0.7} T_{\mathrm{reion}} \left[\frac{1}{h\sqrt{\Omega_0}} \frac{\Omega_{\mathrm{b}} h^2}{0.0125}\right] \quad (16)$$

where $\rho_{\mathrm{c}100}$ is the critical density today if $H_0 = 100$ km s^{-1} Mpc^{-1}, T_{reion} is given by equation (10) and R is the recombination rate given in equation (12) (note that the combination $RT^{0.7}$ is independent of temperature) and Ω_{b}, Ω_0, h and H_0 are cosmological parameters as explained in the Introduction. Note also that temperature is measured in kelvin and B has the dimension of $\mathrm{K}^{1.7}$, hence the factor $\mathrm{K}^{0.7}$ in the last expression.

Integrating equation (15), we obtain

$$T_0^{1.7} = \left(\frac{a_{\mathrm{reion}}^2}{a^2} T_{\mathrm{reion}}\right)^{1.7} + \frac{1.7}{1.9} a^{-3/2}\left[1 - \left(\frac{a_{\mathrm{reion}}}{a}\right)^{1.9}\right] B. \quad (17)$$

The initial condition is chosen such that $T = T_{\mathrm{reion}}$ (equation 10) at $a = a_{\mathrm{reion}}$, the epoch of reionization. An asymptotic limit $a \gg a_{\mathrm{reion}}$ of this equation was first deduced by Miralda-Escudé & Rees (1994).

The equation of evolution for $\gamma - 1$ can be derived from equation (11) by expanding T as in equation (13) and collecting terms that are first order in δ:

$$\frac{\mathrm{d}(\gamma - 1)}{\mathrm{d}a} + (\gamma - 1)\left[\frac{\Omega_z^{0.6}}{a} + 1.7 \frac{\mathrm{d}\ln a^2 T_0}{\mathrm{d}a}\right] = \frac{\mathrm{d}\ln a^2 T_0}{\mathrm{d}a} + \frac{2}{3}\frac{\Omega_z^{0.6}}{a}. \quad (18)$$

In deriving the above, we have made use of the fact that the linear growth factor D_+, which controls the growth of δ for small δ ($\delta \propto D_+$), obeys the relation $\mathrm{d}\ln D_+/\mathrm{d}\ln a = \Omega_z^{0.6}$ (Peebles 1980), where Ω_z is the ratio of matter density to critical density at redshift z. For sufficiently high redshifts, Ω_z approaches 1, which is an approximation we will adopt from now on. This is an excellent approximation at $z \sim 3$ for flat cosmological models. For instance, if the Universe is flat and $\Omega_0 = 0.3$, then $\Omega_z = 0.96$ at $z = 3$. The approximation is somewhat worse for open universe models. For an open universe with $\Omega_0 = 0.3$, $\Omega_z = 0.63$ at $z = 3$. Our results, therefore, will need to be corrected for open universe models. Of course, for models with critical matter density, $\Omega_z = 1$ at any redshift.

Equation (18) is a linear ordinary differential equation for γ, which is straightforward, if somewhat tedious, to solve. Recalling that T_{reion} is independent of δ, we use the initial condition $\gamma - 1 = 0$ at $a = a_{\mathrm{reion}}$ and obtain

$$\gamma - 1 = \frac{1}{1.7}\left[1 - \left(\frac{a_{\mathrm{reion}}^2 T_{\mathrm{reion}}}{a^2 T_0}\right)^{1.7} \frac{a_{\mathrm{reion}}}{a}\right] + \left(\frac{2}{3} - \frac{1}{1.7}\right)(a^2 T_0)^{-1.7} C, \quad (19)$$

where C is defined by

$$C \equiv \frac{1.7}{1.9} B \left\{\frac{a^{1.9}}{2.9}\left[1 - \left(\frac{a_{\mathrm{reion}}}{a}\right)^{2.9}\right] - a_{\mathrm{reion}}^{1.9}\left(1 - \frac{a_{\mathrm{reion}}}{a}\right)\right\} + (a_{\mathrm{reion}}^2 T_{\mathrm{reion}})^{1.7}\left(1 - \frac{a_{\mathrm{reion}}}{a}\right), \quad (20)$$

where B and T_0 are defined in equations (16) and (17). The slope $\gamma - 1 = \mathrm{d}\ln T/\mathrm{d}\ln(1+\delta)$ exhibits the correct qualitative behaviour found using our semi-analytical computation shown in Fig. 3. We plot in Fig. 4 the evolution of $\gamma - 1$ as given by equation (19) for a number of different a_{reion}. An interesting consequence of the above expression for the slope is a limit as to how steep the temperature–density relation can be (or an upper limit to $\gamma - 1$). In the limit

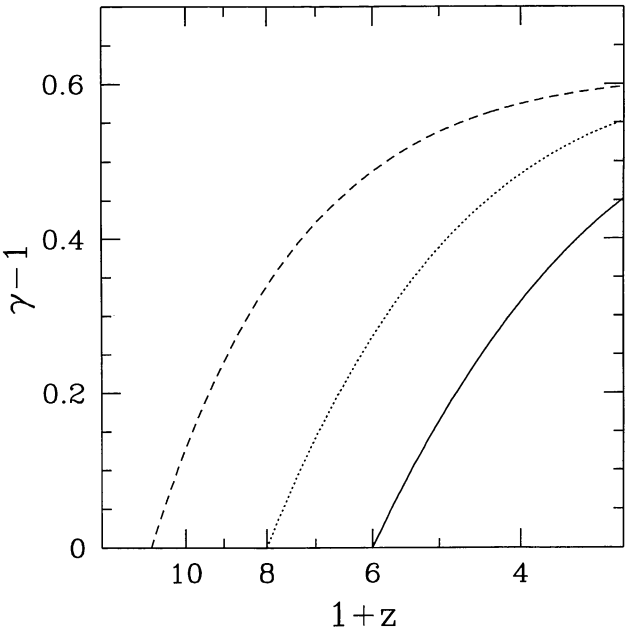

Figure 4. The evolution of $\gamma-1$ as given by equation (19) for $a_{\rm reion}=1/6$ (solid line), $a_{\rm reion}=1/8$ (dotted line) and $a_{\rm reion}=1/11$ (dashed line). Here $T_{\rm reion}=20\,000$ K and $\Omega_0=1$ in all cases.

where reionization occurs very early,

$$\gamma_{\rm max}-1=0.62. \tag{21}$$

This has interesting implications for the slope of the column density distribution of the Lyα forest, which we will discuss in Section 5.

We show in Fig. 5 a comparison of the above expression (equations 13, 17 and 19) with the temperature–density relation obtained by solving numerically the rate equations as outlined in Section 2.1. The evolution of the slope is quite accurately captured by our analytical approximation in equation (19). However, the amplitude T_0 predicted by equation (17) is off: the overall predicted temperature is lower than what it actually is and the predicted spread in T_0 from $z=2$ to $z=4$ is also larger than what the semi-analytical calculation shows (Fig. 5b). This is mainly because helium is not taken into account at all in the above treatment. By ignoring heating arising from photoionization of helium, we systematically underestimate T_0 in our analytical calculation. The time evolution for T_0 is also not quite right for the same reason. We therefore introduce the following modification of equation (17) that gives an excellent fit to the results of the semi-analytical calculations shown in Fig. 3:

$$T_0^{1.7}=\left(\frac{a_{\rm reion}^2}{a^2}\tilde{T}_{\rm reion}\right)^{1.7}+\frac{1.7}{1.9}a^{-[3/2+(a-0.25)/a]}\left[1-\frac{a_{\rm reion}^{1.9}}{a}\right]B,$$

$$\tilde{T}_{\rm reion}=24\,000\ {\rm K} \tag{22}$$

where we have modified the power index of a in the second term on the right-hand side and used $\tilde{T}_{\rm reion}=24\,000$ K, in place of $T_{\rm reion}$ given in equation (10). In general, a different best-fitting $\tilde{T}_{\rm reion}$ would have to be chosen for different abundances of the helium species, when one varies the spectrum

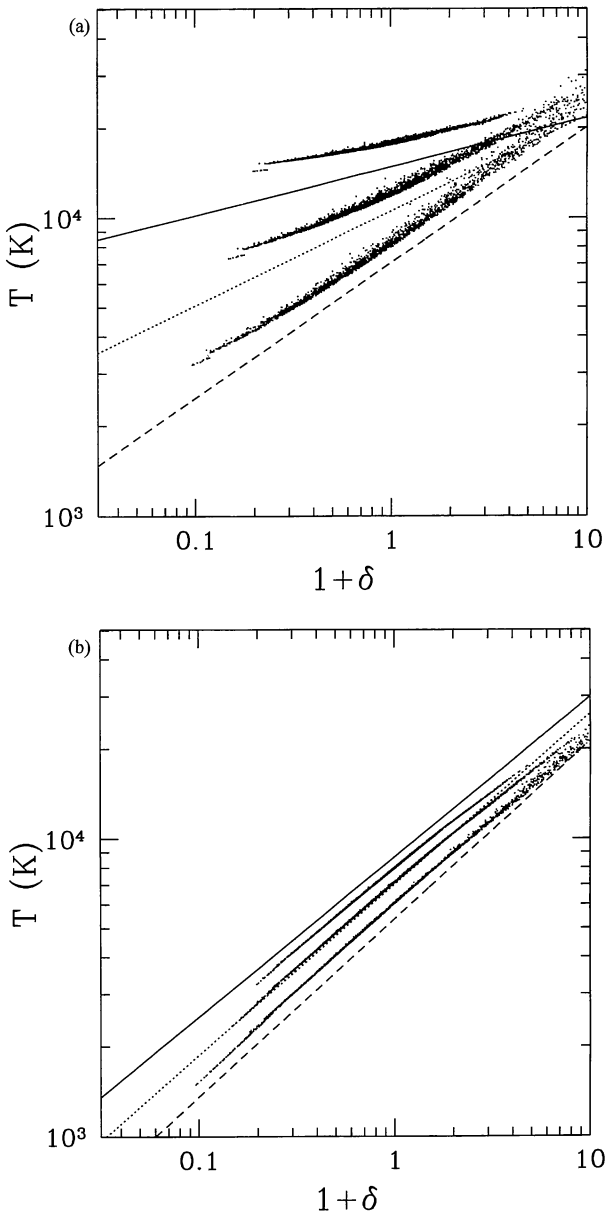

Figure 5. Temperature–density relation for two sudden-reionization models: comparison of results of semi-analytical calculations (black dots) and predictions based on analytical approximations expressed in equations (13), (17) and (19) (solid, dotted and dashed lines). The model parameters are described in the caption of Fig. 3. The black dots in the upper panel and lower panel are exactly the same points as those in Figs 3(a) and (c) respectively, i.e. sudden reionization at $z=6$ and $z=19$. From top to bottom for each figure, the results are shown at $z=4$, 3 and 2 respectively for the black dots and also for the lines. Notice how the predicted slopes match quite well while the amplitudes are off. A modified version of equation (17) (equation 22) gives much better fit to the amplitudes and is used instead in the rest of this paper.

of the ionizing radiation, for instance. We will return to this point later.

On the other hand, the slope of the equation of state $\gamma-1$ is quite insensitive to the exact value of $T_{\rm reion}$, and using the original estimate (equation 10) in equation (19) is sufficiently accurate.

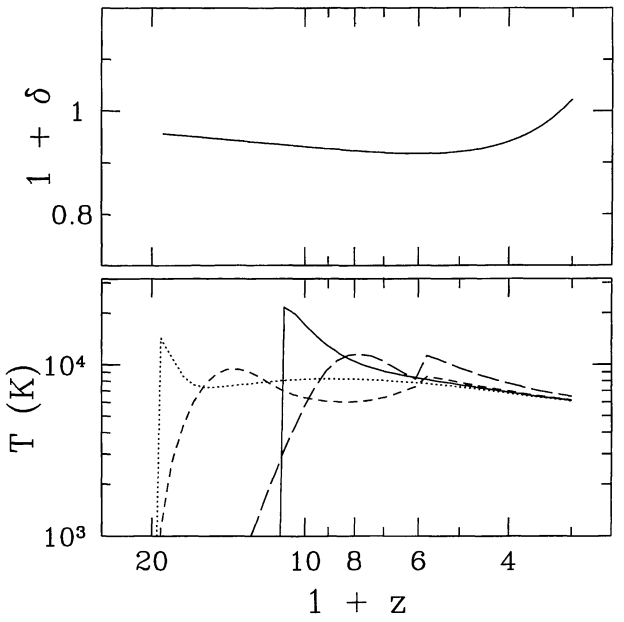

Figure 6. Examples of convergence towards an asymptotic state. In the upper panel is shown the evolution of the overdensity of a fluid element as a function of redshift. In the lower panel is shown the evolution of temperature for the same fluid element, but for a variety of reionization histories. The solid and dotted lines both correspond to sudden reionization models in which $a_{\rm reion}=1/11$ and $a_{\rm reion}=1/20$ respectively and $J_{\rm ion}=0.5$ in equation (6). Their reionization and cosmological parameters are exactly the same as those in Figs 3(c) and (d) respectively. The short-dashed and long-dashed lines correspond exactly to the reionization models shown in Figs 10(a) and (b) respectively, i.e. reionization-proceded-by-reheating models with $a_{\rm heat}=1/20$, $a_{\rm ion}=1/6$, $J_{\rm ion}=0.5$ and $J_{\rm heat}=0.1$ for short-dashed line and $J_{\rm heat}=0.001$ for long-dashed line (see equation 23). The cosmological parameters for these two latter models are the same as those for the solid and dotted lines.

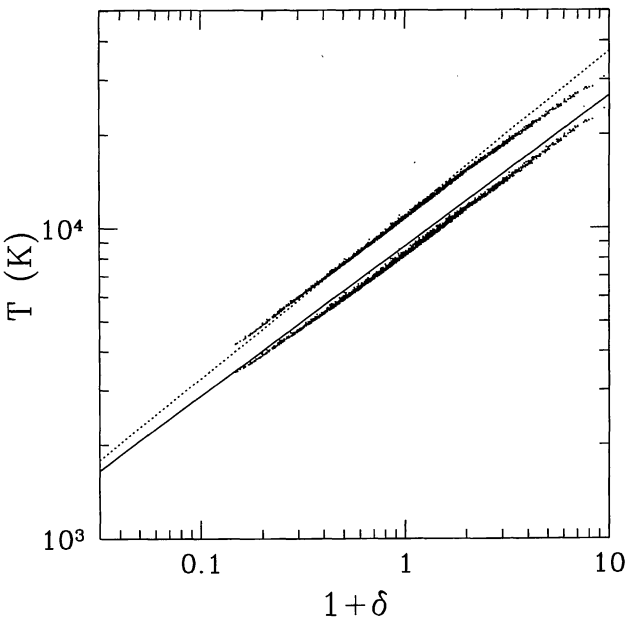

Figure 7. The temperature–density relations for $\Omega_{\rm b}h^2=0.025$ (upper black dots) and $\Omega_{\rm b}h^2=0.0125$ (lower black dots) at $z=3$ for sudden reionization model with radiation turn-on at $z=7$. The rest of the cosmological parameters are exactly the same as those given in Fig. 3. The dotted and solid lines are the predictions according to equations (13), (19) and (22), respectively for the two models.

The analytical predictions for the equation of state shown in Fig. 3 are based on this modified version of T_0 (equation 22) together with equations (13) and (19). Note that, for the case in which the universe reionizes at $z=19$, the temperature–density relation is very close to that of the case in which the universe reionizes at $z=10$. This turns out to be a general trend, that there is an asymptotic temperature–density relation when the universe reionizes sufficiently early. To see how this asymptotic state is approached, we show in Fig. 6 the evolution in temperature of one particular fluid element for different reionization histories. Notice how the solid line (sudden reionization at $z=10$) and the dotted line (sudden reionization at $z=19$) converge. The other lines in the figure correspond to reionization models that will be discussed later. We also find that fluid elements at other densities also exhibit the same kind of convergence towards an asymptotic state.

The expressions in equations (13), (19) and (22) are derived by ignoring processes like Compton cooling that are important at higher redshifts, if the universe is already reionized by then. Hence, the analytical expressions are not quite as accurate for $a_{\rm reion}<1/11$. However, we can make use of the knowledge of asymptotic behaviour for early reionization models and use simply the $a_{\rm reion}=1/11$ result of equations (13), (19) and (22) for any models in which reionization occurs earlier than $z=10$. This is what we have done in making Fig. 3(d).

We now turn to two other interesting variations of the sudden-reionization models.

3.2 Variation with cosmology

We investigate the temperature–density relations for different cosmological parameters, including the baryon density, the Hubble constant and the fraction of critical density in matter. One example is shown in Fig. 7, where $\Omega_{\rm b}h^2$ has been increased by a factor of 2 from the value in Fig. 3. Once again, we find that a power-law equation of state gives an adequate description of the temperature–density relation. Moreover, the analytical expressions in equations (13), (19) and (22) work quite well in describing the change in amplitude and slope. As predicted by equations (22) and (16), the overall temperature increases as $\Omega_{\rm b}h^2$ is raised because the rate of photoionization heating is increased. (Recombination cooling rate is actually also increased but photoionization heating is the dominant entropy changing process.)

We have also tried other variations such as lowering Ω_0. A realistic structure formation model such as the cosmological constant dominated cold dark matter model with $\Omega_0=0.35$ and $h=0.7$ (Kofman, Gnedin & Bahcall 1993; Ostriker & Steinhardt 1995) does not give a very different temperature–density relation from the ones shown in Fig. 3 (using the same $\Omega_{\rm b}h^2$). This can be understood from equations (22) and (16), where it is clear the overall temperature to the 1/1.7th power is dependent upon the combination $h\sqrt{\Omega_0}$ that only varies from 0.5 for the model in Fig. 3 to about 0.4 in the cosmological constant model.

In general, we find that equations (13), (19) and (22) give an agreement to the actual temperature–density relation to within 20 per cent for a variety of cosmological models we have tested. A large part of this error has to do with the fact that changing Ω_0 and h changes the amount of time helium photoionization heating or recombination cooling has to act to make a difference to the thermal evolution. The effect of helium is what we will discuss next.

3.3 Variation with amplitude and spectrum of radiation

The last set of tests we perform for the class of sudden-reionization models is to vary the spectrum and amplitude of the ionization radiation. We find that varying the amplitude of the ionization radiation does not affect the temperature–density relation significantly, as predicted by equations (19) and (22), as long as the flux level is sufficient to keep the universe highly ionized. This is shown in Figs 8(a) and (b), which corresponds to choosing $J_{\rm ion}=0.1$ and 2.0 respectively in equation (6). A comparison of the two figures reveals a slight decrease in temperature when $J_{\rm H\,I}$ is raised, which is a result of more opportunities for recombination cooling, but the effect is very small and becomes insignificant at lower redshifts ($z=2$).

The main effect of varying the spectrum (when fixing $J_{\rm H\,I}$ defined in equation 5) is that one changes the relative abundance of the different species of helium, which could have a non-negligible effect on the temperature owing to recombination cooling and photoionization heating of the various species. We test this effect by varying the He II cut-off factor f in equation (7). Two examples are shown in Fig. 9 where we replot the lines in Fig. 3(a) (that match the temperature–density relations for $f=0.01$ quite well) together with the result of two semi-analytical calculations for $f=1.00$ and $f=10^{-4}$ respectively. By decreasing f, or the amount of radiation energetic enough to ionize He II, one decreases the photoheating rate arising from the ionization of He II into He III, thereby lowering the overall temperature. The reverse happens when f is raised. The change in temperature resulting from this effect could be as large as 20 per cent, with less change as one goes to lower redshift, for a fixed reionization history. One can compensate the error in the analytical estimate of T_0 (which ignores the effect of helium) by lowering/raising $\tilde{T}_{\rm reion}$ in equation (22) as one decreases/increases f (for instance, choosing $\tilde{T}_{\rm reion}=28\,000$ for the $f=1$ case and $\tilde{T}_{\rm reion}=22\,000$ for the $f=10^{-4}$ works reasonably well.)

The power-law slope, on the other hand, does not vary significantly with the spectrum of the ionizing background. It can be seen from Fig. 9 that there is a slight decrease of slope for the corresponding redshifts as one lowers f. This is due to the fact that He II recombination cooling has a stronger effect at higher density. The analytical prediction for the slope in equation (19) works best when the effect of helium is negligible, as can be seen from the better match of slopes for the $f=1$ case. Nevertheless, on the whole, we find that the prediction of equation (19) for the slope is quite robust.

To summarize the results of this section, we find that the temperature–density relation at z of 2 to 4 for sudden-reionization models is well described by a power-law equation of state, with a scatter that depends on the total number of fluid elements. The overall amplitude decreases and the slope steepens as the epoch of reionization is pushed earlier, but the equation of state rapidly approaches an asymptotic limit for reionization occurring at redshifts beyond 10. Quantitative estimates for the slope and ampli-

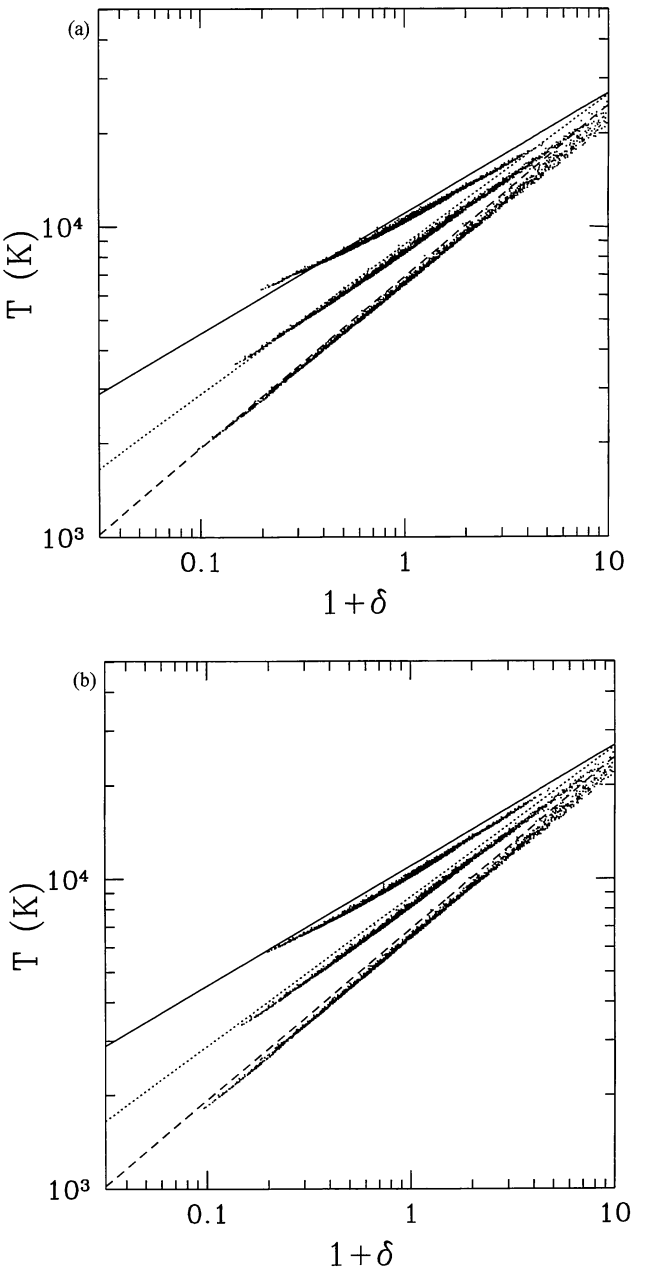

Figure 8. The effect of varying the amplitude of J_ν on the temperature–density relation. Black points in the upper panel (a) are the result of semi-analytical calculation of sudden reionization at $a_{\rm reion}=1/8$ with $J_{\rm ion}=0.1$ (equation 6) while those in the lower panel (b) has $J_{\rm ion}=2.0$ starting from the same $a_{\rm reion}$. The spectrum is chosen to be the same with $f=0.01$ (equation 7) for both panels. The outputs from top to bottom are at $z=4$, 3 and 2. The same solid, dotted and dashed lines are drawn for both panels to facilitate comparison. They are also exactly the same as the lines in Fig. 3(b), based on the analytical expressions in equations (13), (19) and (22), using $a_{\rm reion}=1/8$. The cosmological parameters in Fig. 7 are exactly the same as those in Fig. 3.

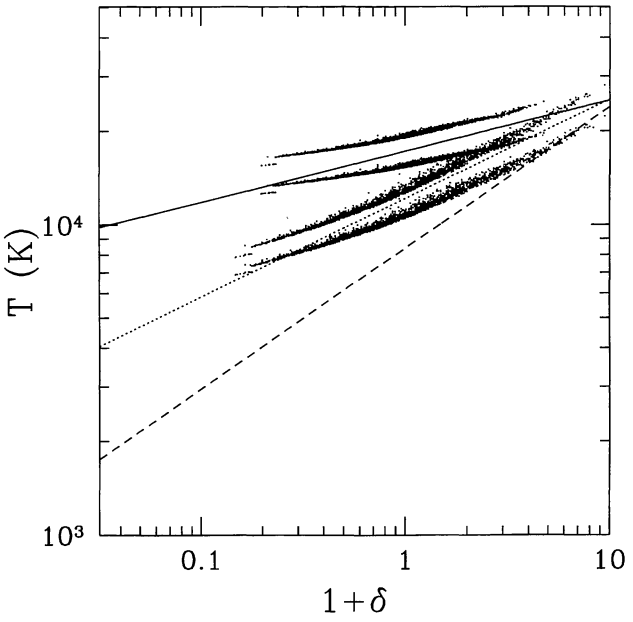

Figure 9. The effect of varying radiation spectrum on the temperature–density relation. Black dots are the results obtained by the semi-analytical calculation explained in Section 2.1. The reionization and cosmological model here is, except for the spectrum, exactly the same as that in Fig. 3(a) where the universe reionizes suddenly at $z=6$. The solid, dotted and dashed lines of Fig. 3(a) are reproduced here for comparison. Above and below the solid line at the top are two sets of points at $z=4$ which correspond to choosing $f=1.0$ (less He II) and $f=10^{-4}$ (more He II) respectively in equation (7). The same is also true for the two sets of points surrounding the dotted line, except that they are at $z=3$. Results are not shown for $z=2$ because the two different fs give significantly overlapping results that are well-represented by the dashed line. The amplitude $J_{\rm H\,I}=0.5$ (equation 5) is adopted throughout.

tude are given in equations (19) and (22). While the analytical prediction for the slope is relatively robust for various cosmologies and spectra, the prediction for the amplitude agrees with the results of the semi-analytical calculations (outlined in Section 2.1) to within 20 per cent for a reasonable range of cosmological and ionization parameters. Most of the error comes from the neglect of helium in obtaining the analytical estimate, which can be compensated if one allows $\bar{T}_{\rm reion}$ to change in equation (22) according to the abundance of the helium species (Fig. 9).

4 REIONIZATION PRECEDED BY REHEATING

The idealization of sudden reionization in the last section allows us to understand the various trends of the temperature–density relation analytically. It is quite possible that the ionizing radiation is turned on more gradually in nature. In particular, we focus on a class of models in which radiation is turned on at some early time, with an intensity large enough to heat up the intergalactic medium but small enough so that the neutral fractions remain high (large recombination rates) although slowly decreasing. This is motivated by hydrodynamic simulations (see Gnedin & Ostriker 1997) in which collapsed regions of high density (that could be stars/quasars) are assumed to give out radiation. As the formation rate of these regions increases with time and the neutral fraction drops steadily, the ionizing intensity climbs until at some point, the universe becomes highly ionized (neutral fraction of hydrogen less than 10^{-4}), thus completing the reionization process when the radiation levels off and species abundances are simply given by the ionization equilibrium. The simulation shown in Figs 1(a) and 2 is one such example.

To investigate the implications of these reionization models systematically, we adopt the following parametrization for the evolution of the ionizing radiation:

$$J_{\rm H\,I}=\begin{cases} J_{\rm ion} & \text{for } a\geq a_{\rm ion},\\ J_{\rm heat}(a/a_{\rm ion})^7 & \text{for } a_{\rm ion}>a\geq a_{\rm heat},\\ 0 & \text{for } a_{\rm heat}>a,\end{cases} \tag{23}$$

where $J_{\rm H\,I}$ is defined in equation (5), $a_{\rm heat}$ and $a_{\rm ion}$ denote the size of the Hubble scalefactor at the onset of reheating and reionization. The slope a^7 in the second row of equation (23) comes from fitting $J_{\rm H\,I}(a)$ in Fig. 2. The spectrum of J_ν is assumed to have the same form as in equation (7) with $f=0.01$ and J_0 chosen to match whatever $J_{\rm H\,I}$ is specified above.

Before discussing the results for these models, let us point out that in Fig. 1, we have already shown an example of the temperature–density relation of a reionization-preceded-by-reheating model where J varies with time as in Fig. 2. Notice how the temperature–density relation can be approximated by an equation of state resulting from a sudden reionization model (the solid line in Fig. 1). The same turns out to be true for all other reionization models we have tested, with the parametrization given in equation (23).

Two interesting examples are shown in Fig. 10. Both have the same epochs of reheating and reionization ($a_{\rm heat}$ and $a_{\rm ion}$). The only difference is the amount of reheating that occurs: $J_{\rm heat}$ being 0.001 versus 0.1 in equation (23). They can both be approximately fitted with sudden reionization models (no preceding reheating period) where the epoch of sudden reionization is chosen to lie somewhere between $a_{\rm heat}$ and $a_{\rm ion}$. The larger the amount of reheating, the earlier the epoch of reionization is required. It is also interesting to note that in Fig. 10(a), the fit to the result at $z=4$ is not as good as those at $z=3$ or $z=2$. It is because it takes some time for the universe to settle to its asymptotic state (i.e. a state which is independent of prior history, whether it be sudden reionization, gradual reionization with preheating, etc.). The same should also be true for Fig. 10(b), except that because the amount of preheating is more significant, the universe, in effect, has more time to settle to its asymptotic state, hence the better agreement with sudden reionization models for all three redshifts.

To illustrate this convergence towards an asymptotic state, we show in Fig. 6 the evolution of temperature for one particular fluid element for four different reionization histories. The tendency to approach the same limiting temperature, for a given density evolution, can be clearly seen. Note how the model illustrated with a long-dashed line evolves to a temperature a little higher than the others, by $z=2$. This is because of its relatively small amount of reheating (small $J_{\rm heat}$ in equation 23) that implies the universe

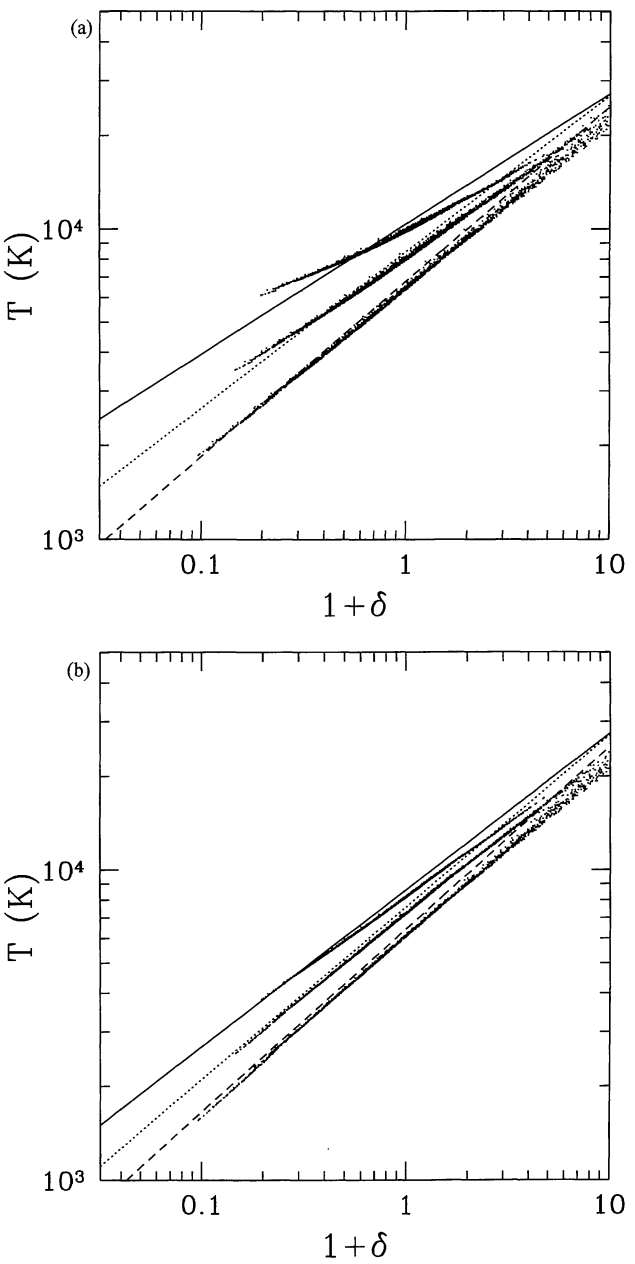

Figure 10. Black dots in (a) (upper panel) show the temperature–density relation for a reionization model in which $a_{\rm heat}=1/20$, $a_{\rm ion}=1/6, J_{\rm heat}=0.001$ and $J_{\rm ion}=0.5$ (see equation 23). The three sets of points are from top to bottom at $z=4$, 3 and 2. The solid, dotted and dashed lines are analytical approximations of sudden reionization models expressed in equations (13), (19) and (22), choosing $a_{\rm reion}=1/8.4$. (b) In the lower panel, on the other hand, corresponds to the choice of parameters $a_{\rm heat}=1/20$, $a_{\rm ion}=1/6$, $J_{\rm heat}=0.1$ and $J_{\rm ion}=0.5$ in equation (23). The analytical approximations shown have $a_{\rm reion}$ equal to 1/10 in equations (13), (19) and (22). For both (a) and (b) the cosmological model is the same as that in Fig. 3.

effectively reionizes at a later redshift, giving it less time to settle to its asymptotic state.

We have tested several other reionization models where all the parameters in equation (23) are varied systematically. The same conclusion holds for all of them, namely that a sudden-reionization model (no preceding reheating) can always be found to fit the temperature–density relation of any reionization model with reheating, with the turn-on redshift of the former chosen somewhere between the epochs of reheating and reionization of the latter.

5 DISCUSSION

Let us summarize what we have learned so far.

We find that the temperature–density relation of the low-density intergalactic medium, while having an intrinsic scatter, is well described by a mean equation of state of the form $T=T_0(1+\delta)^{\gamma-1}$. It is shown that any reionization model with gradual radiation turn-on produces equation of state that can be well approximated by one produced by a suitably chosen sudden turn-on model (Section 4).

In general, the mean temperature T_0 at $\delta=0$ at a given redshift $z\sim2$–4 decreases as the epoch of reionization is pushed earlier. It is only weakly dependent on the amplitude of the ionizing flux $J_{\rm H\,I}$ at $z\sim2$–4 assuming reionization takes place at $z\gtrsim5$. The spectrum of J_ν can introduce an about 20 per cent change to T_0. Its main effect is on the abundances of helium species, affecting the amount of photoionization heating and recombination cooling. Cosmological parameters change T_0 in a simple way: for sufficiently early reionization, $T_0\propto(\Omega_{\rm b}h/\sqrt{\Omega_0})^{1/1.7}$. All the dependences mentioned above are expressed in a quantitative way in equation (22), with about 20 per cent accuracy depending on the spectrum of J_ν and cosmology.

The slope of the equation of state, $\gamma-1$, increases with redshift and with earlier reionization epoch (equation 19 and Fig. 4). Its evolution is only weakly dependent on cosmology. There exists a maximum as to how steep $\gamma-1$ can become, which is about 0.62 (equation 21). Strictly speaking, $\gamma-1$ can be as small as 0 right at the onset of sudden reionization, but for reionization occurring earlier than $z_{\rm reion}\sim5$, it is greater than 0.3 at $z=3$; for $z_{\rm reion}>7$ the minimum γ is about 0.47.

What do all these imply for the observable properties of the low column density Lyα forest? First, for a given density (or $1+\delta$) profile and the Hubble constant h, the column density it corresponds to is proportional to $\Omega_{\rm b}^2T^{-0.7}J_{\rm H\,I}^{-1}$. Uncertainty in the reionization history introduces an about 50 per cent uncertainty in T (see Fig. 3), which in turn implies an about 30 per cent uncertainty in column density. This means an additional uncertainty in the amplitude of the column density distribution on top of that owing to $\Omega_{\rm b}$ and $J_{\rm H\,I}$, even if one is given a known cosmological model (Hui et al. 1997).

Note that for sufficiently early reionization, the dependence $T_0\propto\Omega_{\rm b}^{1.7}$ implies that the column density is scaled by $\Omega_{\rm b}^{2-0.7/1.7}=\Omega_{\rm b}^{1.6}$, which is roughly consistent with the result of Croft et al. (1996), who found $\Omega_{\rm b}^{1.7}$ scaling using hydrodynamic simulations.

The good news, on the other hand, is that the slope of the column density distribution is relatively independent of the equation of state of the intergalactic medium. The slope of the column density distribution (number of absorption lines per unit column density per unit redshift $\propto N_{\rm H\,I}^{-\beta}$ where $N_{\rm H\,I}$ is the column density) is approximately given by

$$\beta=1+\frac{0.96-0.8(\sigma_0-1)-0.4(n_{\rm eff}+2.33)}{1.68-0.7(\gamma-1)}, \qquad (24)$$

where σ_0 is the rms mass fluctuation at scales close to the Jeans length and $n_{\rm eff}$ is the effective slope of the power spectrum at the same scales. They are close to 1 and -2.33 respectively, but their precise values are determined by the cosmological model. The form of the above expression can be deduced by relating the column density distribution of absorption lines to a statistic of density peaks, and assuming the validity of the Zel'dovich approximation. The reader is referred to Hui et al. (1997) for details. Taking the range of $\gamma-1$ from 0.3 to 0.62 we have derived previously, the uncertainty in β introduced by unknown reionization history is of the order of 7 per cent.[2]

This is a very important conclusion because the slope of column density distribution then becomes a powerful discriminant of cosmological models through σ_0 and $n_{\rm eff}$. It is relatively free of uncertainties in the temperature–density relation of the intergalactic medium, or the values of $\Omega_{\rm b}$ and $J_{\rm H\,I}$, unlike the amplitude of the column density distribution. The reader is referred to Hui et al. (1997) for a more detailed discussion of the predictions of various cosmological models for β.

The temperature–density relation also has significant implications for the b parameter distribution. There exists a rather sharp lower cut-off of about $b=20$ km s^{-1} according to high-resolution data of the low column density Lyα observation (Hu et al. 1995). If one naively assumes the observed b is completely a result of thermal broadening $b=\sqrt{2kT/m_{\rm p}}$, one obtains a lower cut-off temperature of about 24 000 K. Judging from Fig. 3, it is clear that at $z\sim3$, which is the relevant redshift for these observations, unless the universe reionizes much later than $z=5$, all the underdense regions (and including some overdense regions too, depending on the reionization history) have lower temperature than this cut-off. This is true even if one allows for a lot of helium photoionization heating or very little helium recombination cooling by varying the spectrum (see Fig. 9). There are a few possible resolutions: first, it is possible that the low column density objects that we observe (column density lower than about 10^{15} cm^2) actually correspond to higher densities (δ), but that would imply a very high $J_{\rm H\,I}$ (higher than about 20) that is difficult to reconcile with observations (see Hui et al. 1997); secondly, it could be that the universe is not photo-reionized after all and some other mechanism is at work; thirdly, the observed b parameter for these low column density systems is not the result of thermal broadening alone. We consider the last possibility the most likely one. As we have argued in an earlier paper (Hui et al. 1997) and was pointed out before by numerous authors (see for instance Cen et al. 1994; Hernquist et al. 1996; Miralda-Escudé et al. 1996; Zhang et al. 1995), the observed absorption profiles do not necessarily conform to the classic Voigt profile but can instead reflect more the underlying mass density profile and peculiar velocity structure. For instance, a structure collapsing perpendicular to the line of sight (thus having density enhancement to induce enhanced absorption) can have an expanding velocity component along the line of sight, thus creating a profile broader than what naive thermal broadening would predict.

[2]The reionization history, in addition to affecting γ, can actually also influence σ_0 through its dependence on the Jeans scale. We expect the effect to be small for sufficiently early reionization.

Finally, let us speculate on how a fluctuating ionizing field might change the results of our paper. From Fig. 9, it is clear that a fluctuating field with inhomogeneous spectrum can certainly introduce a lot of scatter to the temperature–density relation, by giving different photoionization heating and recombination cooling rates even for fluid elements with the same density evolution. Moreover, the ionizing field can also turn on at different times for different fluid elements because of radiative transfer effects (Zuo 1992a,b). This would introduce additional scatter because as we have seen, the earlier the reionization epoch, the lower the temperature at a given redshift.

However, we also learn that the temperature–density relation approaches an asymptotic limit if one waits long enough. For sufficiently early reionization, neither the amplitude of $J_{\rm H\,I}$ nor the reionization history (e.g. at what different times radiation turns on at different elements) affects the temperature very much, assuming $J_{\rm H\,I}$ is large enough to keep the universe reionized (see Section 3.3). Therefore, provided the amplitude of J_ν at the helium ionizing frequencies does not vary significantly with position at later times $z\sim2$–4, the equation of state we calculate for the early reionization models should be valid, even if the amplitude of $J_{\rm H\,I}$ fluctuates at $z\sim2$–4. This certainly warrants further research, which we will leave for future work.

ACKNOWLEDGMENTS

We are grateful to Martin Rees, Jordi Miralda-Escudé and our anonymous referee for valuable comments and suggestions that considerably improved the manuscript. This work was supported in part by the DOE and by the NASA (NAGW-2381) at Fermilab and by the UC Berkeley grant 1-443839-07427. Simulations were performed on the NCSA Power Challenge Array under the grant AST-960015N. NG is grateful to Joshua Frieman and the Theoretical Astrophysics group at Fermilab for hospitality, where part of this work was completed.

REFERENCES

Aldrovandi S. M. V., Pequignot D., 1973, A&A, 25, 137
Bartelmann M., Schneider P., 1992, A&A, 259, 413
Bertschinger E., Jain B., 1994, ApJ, 431, 486
Bi H. G., Borner G., Chu Y., 1992, A&A, 266, 1
Bi H. G., Davidsen A. F., 1997, ApJ, 479, 523
Black J. H., 1981, MNRAS, 197, 553
Burgess A., Seaton M. J., 1960, MNRAS,, 121, 471
Cen R., 1992, ApJS, 78, 341
Cen R. Y., Miralde-Escudé J., Ostriker J. P., Rauch M. R., 1994, ApJ, 437, L9
Coles P., Melott A. L., Shandarin S. F., 1993, MNRAS, 260, 765
Couchman H. M. P., Rees M. J., 1986, MNRAS, 221, 53
Cristiani S., D'Odorico S., D'Odorico V., Fontana A., Giallongo E., Savaglio S., 1997, MNRAS, 285, 209
Croft R. A. C., Weinberg D. H., Katz N., Hernquist L., 1996, ApJ, submitted (astro-ph 9611053)
Doroshkevich A. G., 1970, Afz, 6, 581
Doroshkevich A. G., Shandarin S., 1977, MNRAS, 179, 95
Ferland G. J., Peterson B. M., Horne K., Welsh W. F., Nahar S. N., 1992, ApJ, 387, 95
Giroux M. L., Shapiro P. R., 1996, ApJS, 102, 191
Gnedin N. Y., 1995, ApJS, 97, 231

Gnedin N. Y., Bertschinger E., 1996, ApJ, 470, 115
Gnedin N. Y., Hui L., 1996, ApJ, 472, L73
Gnedin N. Y., Ostriker J. P., 1997, ApJ, 486, 581
Gunn J. E., Peterson B. A., 1965, ApJ, 142, 1633
Haiman Z., Loeb A., 1996, ApJ, submitted (astro-ph 9611028)
Haardt F., Madau P., 1996, ApJ, 461, 20
Hernquist L., Katz N., Weinberg D. H., Miralde-Escudé J., 1996, ApJ, 457, L51
Hu E., Kim T., Cowie L. L., Songalia A., 1995, AJ, 110, 1526
Hui L., Gnedin N. Y., Zhang Y., 1997, ApJ, 486, 599
Ikeuchi S., Ostriker J. P., 1986, ApJ, 301, 522
Kofman L. A., Gnedin N. Y., Bahcall N. A., 1993, ApJ, 413, 1
Lotz W., 1967, ApJS, 14, 207
Lu L., Sargent W. L. W., Womble D. S., Takada-Hidai M., 1996, ApJ, 472, 509
Meiksin A., Madau P., 1993, ApJ, 412, 34
Miralda-Escudé J., Cen R., Ostriker J. P., Rauch M., 1996, ApJ, 471, 582
Miralda-Escudé J., Ostriker J. P., 1992, ApJ, 392, 15
Miralda-Escudé J., Rees M. J., 1994, MNRAS, 266, 343
Ostriker J. P., Steinhardt P. J., 1995, Nat, 377, 600
Peebles P. J. E., 1980, The Large Scale Structure of the Universe. Princeton Univ. Press, Princeton
Peebles P. J. E., 1993, Principles of Physical Cosmology. Princeton Univ. Press, Princeton
Reisenegger A., Miralda-Escudé J., 1995, ApJ, 449, 476
Sciama D. W., 1990, ApJ, 364, 549
Shapiro P. R., 1995, in Ferrara A. et al., eds, ASP Conf. Ser. Vol. 80, The physics of the interstellar and intergalactic matter. Astron. Soc. Pac., San Francisco, p. 113
Shapiro P. R., Giroux M. L., Babul A., 1994, ApJ, 427, 25
Songaila A., Cowie L. L., 1996, ApJ, 112, 335
Verner D. A., Ferland G. J., Korista K. T., Yakovlev D. G., 1996, ApJ, 465, 487
Wadsley J. W., Bond J. R., 1997, in Clarke D. A., West M. J., eds, ASP Conf. Ser. Vol. 123, Computational astrophysics. Astron. Soc. Pac., San Francisco, p. 332
Zel'dovich Ya. B., 1970, A&A, 5, 84
Zhang Y., Anninos P., Norman M. L., 1995, ApJ, 453, L57
Zuo L., 1992a, MNRAS, 258, 36
Zuo L., 1992b, MNRAS, 258, 45

APPENDIX A: IONIZATION AND RECOMBINATION RATES

In this section we compile the ionization and recombination rates used in our calculations. We believe that this compilation is sufficiently up-to-date to reflect all recent improvements. In some of the equations below the following notation is used:

$$\lambda_j = 2\frac{T_j^{(\mathrm{TR})}}{T},$$

where T is the temperature, and $T_j^{(\mathrm{TR})}$ are ionization thresholds for species $j = \mathrm{H\,I}$, $\mathrm{He\,I}$ and $\mathrm{He\,II}$ expressed in temperature units,

$$T_{\mathrm{H\,I}}^{(\mathrm{TR})} = 157\,807\ \mathrm{K},$$

$$T_{\mathrm{He\,I}}^{(\mathrm{TR})} = 285\,335\ \mathrm{K},$$

$$T_{\mathrm{He\,II}}^{(\mathrm{TR})} = 631\,515\ \mathrm{K}.$$

The symbol k_{B} denotes the Boltzmann constant.

For chemical evolution, we use the symbols *RI*, *CI* and *DI* to denote hydrogen and helium recombination rates, collisional ionization rates and dielectronic recombination rates.

For thermal evolution, we use the symbols *RC*, *CC*, *DC* and *EC* to denote hydrogen and helium recombination cooling, collisional ionization cooling, dielectronic recombination cooling and line excitation cooling rates.

Superscripts and subscripts are added to the above symbols to distinguish between different processes within each class.

Molecular hydrogen and metal cooling are not expected to be important for the low-density intergalactic medium that we are interested in (see Songaila & Cowie 1996 for a discussion of metals detected in the Lyα forest).

Compton cooling rates and the photoionization cross-sections are given at the end.

Case A H II recombination coefficient: our fit to the data from Ferland et al. (1992); accurate to 2 per cent from 3 to 10^9 K:

$$RI^{\mathrm{A}}_{\mathrm{H\,II}} = 1.269\times10^{-13}\ \mathrm{cm^3\ s^{-1}}\ \frac{\lambda_{\mathrm{H\,I}}^{1.503}}{[1.0+(\lambda_{\mathrm{H\,I}}/0.522)^{0.470}]^{1.923}}.$$

Case A H II recombination cooling rate: our fit to the data from Ferland et al. (1992); accurate to 2 per cent from 3 to 10^9 K:

$$RC^{\mathrm{A}}_{\mathrm{H\,II}} = 1.778\times10^{-29}\ \mathrm{erg\ cm^3\ s^{-1}\ K^{-1}}\ T\ \frac{\lambda_{\mathrm{H\,I}}^{1.965}}{[1.0+(\lambda_{\mathrm{H\,I}}/0.541)^{0.502}]^{2.697}}.$$

Case A He II recombination coefficient: from Burgess & Seaton (1960); accurate to $\sim$10 per cent from 5×10^3 to 5×10^5 K:

$$RI^{\mathrm{A}}_{\mathrm{He\,II}} = 3.0\times10^{-14}\ \mathrm{cm^3\ s^{-1}}\ \lambda_{\mathrm{He\,I}}^{0.654}.$$

Case A He II recombination cooling rate: from Burgess & Seaton (1960); accurate to ~10 per cent from 5×10^3 to 5×10^5 K:

$$RC^{\rm A}_{\rm He\,II}=k_{\rm B}T\,RI^{\rm A}_{\rm He\,II}.$$

Case A He III recombination coefficient: our fit to the data from Ferland et al. (1992); accurate to 2 per cent from 1 to 10^9 K:

$$RI^{\rm A}_{\rm He\,III}=2.0\times1.269\times10^{-13}\ {\rm cm^3\ s^{-1}}\,\frac{\lambda_{\rm He\,II}^{1.503}}{[1.0+(\lambda_{\rm He\,II}/0.522)^{0.470}]^{1.923}}.$$

Case A He III recombination cooling rate: our fit to the data from Ferland et al. (1992); accurate to 2 per cent from 1 to 10^9 K:

$$RC^{\rm A}_{\rm He\,III}=8\times1.778\times10^{-29}\ {\rm erg\ cm^3\ s^{-1}\ K^{-1}}\,T\,\frac{\lambda_{\rm He\,II}^{1.965}}{[1.0+(\lambda_{\rm He\,II}/0.541)^{0.502}]^{2.697}}.$$

Case B H II recombination coefficient: our fit to the data from Ferland et al. (1992); accurate to 0.7 per cent from 1 to 10^9 K:

$$RI^{\rm B}_{\rm H\,II}=2.753\times10^{-14}\ {\rm cm^3\ s^{-1}}\,\frac{\lambda_{\rm H\,I}^{1.500}}{[1.0+(\lambda_{\rm H\,I}/2.740)^{0.407}]^{2.242}}.$$

Case B H II recombination cooling rate: our fit to the data from Ferland et al. (1992); accurate to 2 per cent from 1 to 10^9 K:

$$RC^{\rm B}_{\rm H\,II}=3.435\times10^{-30}\ {\rm erg\ cm^3\ s^{-1}\ K^{-1}}\,T\,\frac{\lambda_{\rm H\,I}^{1.970}}{[1.0+(\lambda_{\rm H\,I}/2.250)^{0.376}]^{3.720}}.$$

Case B He II recombination coefficient: from Burgess & Seaton (1960); accurate to ~10 per cent from 5×10^3 to 5×10^5 K:

$$RI^{\rm B}_{\rm He\,II}=1.26\times10^{-14}\ {\rm cm^3\ s^{-1}}\,\lambda_{\rm He\,I}^{0.750}.$$

Case B He II recombination cooling rate: from Burgess & Seaton (1960); accurate to ~10 per cent from 5×10^3 to 5×10^5 K:

$$RC^{\rm B}_{\rm He\,II}=k_{\rm B}T\,RI^{\rm B}_{\rm He\,II}.$$

Case B He III recombination coefficient: our fit to the data from Ferland et al. (1992); accurate to 2 per cent from 3 to 10^9 K:

$$RI^{\rm B}_{\rm He\,III}=2.0\times2.753\times10^{-14}\ {\rm cm^3\ s^{-1}}\,\frac{\lambda_{\rm He\,II}^{1.500}}{[1.0+(\lambda_{\rm He\,II}/2.740)^{0.407}]^{2.242}}.$$

Case B He III recombination cooling rate: our fit to the data from Ferland et al. (1992); accurate to 2 per cent from 3 to 10^9 K:

$$RC^{\rm B}_{\rm He\,III}=8\times3.435\times10^{-30}\ {\rm erg\ cm^3\ s^{-1}\ K^{-1}}\,T\,\frac{\lambda_{\rm He\,II}^{1.970}}{[1.0+(\lambda_{\rm He\,II}/2.250)^{0.376}]^{3.720}}.$$

H I collisional ionization coefficient: our fit to the data from Lotz (1967); accurate to 3 per cent from 10^4 to 10^9 K:

$$CI_{\rm H\,I}=21.11\ {\rm cm^3\ s^{-1}\ K^{3/2}}\,T^{-3.2}\,{\rm e}^{-\lambda_{\rm H\,I}/2}\,\frac{\lambda_{\rm H\,I}^{-1.089}}{[1+(\lambda_{\rm H\,I}/0.354)^{0.874}]^{1.101}}.$$

H I collisional ionization cooling rate: derived from the collisional ionization coefficient:

$$CC_{\rm H\,I}=k_{\rm B}T^{\rm (TR)}_{\rm H\,I}\,CI_{\rm H\,I}.$$

He I collisional ionization coefficient: our fit to the data from Lotz (1967); accurate to 3 per cent from 10^4 to 10^9 K:

$$CI_{\rm He\,I} = 32.38\ {\rm cm^3\ s^{-1}\ K^{3/2}}\ T^{-3/2}\,{\rm e}^{-\lambda_{\rm He\,I}/2}\,\frac{\lambda_{\rm He\,I}^{-1.146}}{[1+(\lambda_{\rm He\,I}/0.416)^{0.987}]^{1.056}}.$$

He I collisional ionization cooling rate: derived from the collisional ionization coefficient:

$$CC_{\rm He\,I} = k_{\rm B} T_{\rm He\,I}^{\rm (TR)} CI_{\rm He\,I}.$$

He II collisional ionization coefficient: our fit to the data from Lotz (1967); accurate to 3 per cent from 10^4 to 10^9 K:

$$CI_{\rm He\,II} = 19.95\ {\rm cm^3\ s^{-1} K^{3/2}}\ T^{-3/2}\,{\rm e}^{-\lambda_{\rm He\,II}/2}\,\frac{\lambda_{\rm He\,II}^{-1.089}}{[1+(\lambda_{\rm He\,II}/0.553)^{0.735}]^{1.275}}.$$

He II collisional ionization cooling rate: derived from the collisional ionization coefficient:

$$CC_{\rm He\,II} = k_{\rm B} T_{\rm He\,II}^{\rm (TR)} CI_{\rm He\,II}.$$

He II dielectronic recombination coefficient: from Aldrovandi & Pequignot (1973); accurate to $\sim$5 per cent from 3×10^4 to 10^6 K:

$$DI_{\rm He\,II} = 1.90\times10^{-3}\ {\rm cm^3\ s^{-1}\ K^{3/2}}\ T^{-3/2}\,{\rm e}^{-0.75\lambda_{\rm He\,III}/2}(1+0.3\,{\rm e}^{-0.15\lambda_{\rm He\,III}/2}).$$

He II dielectric recombination cooling rate: derived from the dielectronic recombination coefficient:

$$DC_{\rm He\,II} = 0.75 k_{\rm B} T_{\rm He\,II}^{\rm (TR)} DI_{\rm He\,III}.$$

H I line excitation cooling rate: from Black (1981) with the correction from Cen (1992); accurate to $\sim$10 per cent from 5×10^3 to 5×10^5 K:

$$EC_{\rm H\,I} = 7.5\times10^{-19}\ {\rm erg\ cm^3\ s^{-1}}\,{\rm e}^{-0.75\lambda_{\rm H\,I}/2}\,\frac{1}{1+(T/10^5\ {\rm K})^{1/2}}.$$

He II line excitation cooling rate: from Black (1981) with the correction from Cen (1992); accurate to $\sim$10 per cent from 5×10^3 to 5×10^5 K:

$$EC_{\rm He\,II} = 5.54\times10^{-17}\ {\rm erg\ cm^3\ s^{-1}}\left(\frac{1\ {\rm K}}{T}\right)^{0.397}{\rm e}^{-0.75\lambda_{\rm He\,II}/2}\,\frac{1}{1+(T/10^5\ {\rm K})^{1/2}}.$$

Compton heating/cooling term in the equation (2) is given by the following expression (Peebles 1993), which is exact in the non-relativistic limit:

$$\frac{{\rm d}Q_{\rm Compton}}{{\rm d}t} = 6.35\times10^{-41}\ {\rm erg\ cm^{-3}\ s^{-1}\ K^{-1}}\,\Omega_{\rm b}h^2\tilde{X}_e(1+z)^7[2.726\ {\rm K}(1+z)-T].$$

Photoionization cross-sections are taken from Verner et al. (1996) in the following form:

$$\sigma(E) = \sigma_0[(x-1)^2+y_w^2]\,\frac{y^{0.5P-5.5}}{(1+\sqrt{y/y_a})^P},$$

where $x = E/E_0 - y_0$ and $y = \sqrt{x^2+y_1^2}$. Quantities $\sigma_0, E_0, y_w, P, y_a, y_0$ and y_1 are fitting parameters and are given in the Table A1. They are accurate to within 10 per cent from the respective ionization thresholds to 5 keV.

Table A1. Photoionization cross-section parameters.

Species	E_0 (eV)	σ_0 (cm^2)	P	y_a	y_w	y_0	y_1
H I	4.298×10^{-1}	5.475×10^{-14}	2.963	32.88	0	0	0
He I	1.361×10^{1}	9.492×10^{-16}	3.188	1.469	2.039	0.4434	2.136
He II	1.720	1.369×10^{-14}	2.963	32.88	0	0	0